Delft University of Technology

Lattice-Boltzmann Numerical Investigation of a Realistic Multi-Cavity Acoustic Liner with Grazing Flow

Meirelles Pereira, L.; Bonomo, Lucas A.; da Silva, Andrey R.; Cordioli, Júlio A.; Avallone, F.

Important note
To cite this publication, please use the final published version (if applicable).
Please check the document version above.

Lattice-Boltzmann Numerical Investigation of a Realistic Multi-Cavity Acoustic Liner with Grazing Flow

Lucas M. Pereira[*], Lucas A. Bonomo[†], Andrey R. da Silva[‡] and Júlio A. Cordioli[§]
Federal University of Santa Catarina, Florianópolis, 88040-900, Brazil

Francesco Avallone[¶]
Delft University of Technology, 2629 HS Delft, The Netherlands

Scaled-resolved numerical simulations using the lattice-Boltzmann Very Large Eddy Simulation method are performed to compute the acoustic impedance of a realistic multi-cavity single degree of freedom liner grazed by a turbulent boundary layer. Numerical results are assessed against experimental impedance measurements carried out in grazing flow impedance test facility at the Federal University of Santa Catarina (UFSC), with three different approaches: the in-situ technique, the mode matching method and a Prony-like algorithm. Both experiments and numerical simulations are carried out with and without turbulent grazing flow at Mach number equal to 0.3 and with grazing acoustic tonal plane wave. Acoustic waves with amplitude equal to 130 dB and 145 dB are analyzed. For each amplitude, six frequencies are investigated in the range between 800 Hz and 2300 Hz. For each case, the acoustic wave propagates both in the same direction and opposite to the grazing turbulent flow. Numerical results show very good agreement with experimental data for the no-flow case. In the presence of grazing flow, preliminary numerical results show an overestimation of the resistance with respect to the experimental data. It has been found that using a less dissipative solver for the acoustic simulations and increasing the resolution lead to better agreement. Nevertheless, the numerical database predicts well the different trends between the impedance measurement methods. The presented database, after being recomputed with the less dissipative solver, will be used to understand the physical reasons behind the different impedance measurement results obtained with different eduction methods and clarify the physics of the flow-acoustic interaction.

I. Introduction

Acoustic liners are passive noise control devices widely used in modern turbofan aircraft engines to mitigate tonal noise, especially at blade passing frequency. They consist of an arrangement of single degree of freedom (SDOF) Helmholtz resonators typically built with a perforated face sheet separated from a rigid back plate by a honeycomb structure. In general, these devices are characterized through the acoustic impedance. However, the presence of grazing flow considerably affects the acoustic response of the liner and the measured impedance. The physics behind the interaction between the acoustic field and the turbulent flow is still not fully understood, and remains a research topic. In this context, high-fidelity numerical simulations have the potential to provide valuable insights into flow-acoustic interaction and non-linear behavior of the liner, which can improve the liner design process.

The liner acoustic impedance depends on many factors, including its geometry, grazing flow velocity, boundary layer parameters, temperature, and both sound pressure level (SPL) and frequency of the incident acoustic wave [1–3]. Given the complexity of the problem, many studies have been carried out in order to investigate the impact of each parameter over the liner's impedance, by means of both numerical and experimental analysis. For example, Tam et al. [4] performed a coupled experimental and numerical study to describe the non-linear behaviour of resonant slit acoustic liners subjected to normal incidence sound waves with high SPL. The conversion of the acoustic energy into rotational kinetic energy in the form of vortices was found to be the dominant mechanism of noise reduction. Afterwards, Tam

---

[*]MSc Student, Department of Mechanical Engineering, lucas.meirelles@lva.ufsc.br, Non AIAA Member.

[†]PhD Student, Department of Mechanical Engineering, lucas.bonomo@lva.ufsc.br, Non AIAA Member.

[‡]Associate Professor, Department of Mechanical Engineering, andrey.rs@ufsc.br, AIAA Member.

[§]Associate Professor, Department of Mechanical Engineering, julio.cordioli@ufsc.br, AIAA Member.

[¶]Assistant Professor, Flow Physics and Technology Department, f.avallone@tudelft.nl, AIAA Member.

et al. [5] performed a 2D direct numerical simulations (DNS) of a slit resonator cavity with grazing laminar flow. Similarly to the no-flow case, vortex shedding was observed as a primary dissipation mechanism of acoustic energy for high SPL incident waves. It was shown that the large scale vortices, ejected from the resonator's orifice, are advected by the grazing flow and interact with downstream cavities, thus potentially affecting the overall drag induced by the liner. On the other hand, low SPL incident acoustic waves were found to be attenuated mainly by viscous effects within the resonator's orifice. Zhang and Bodony [6] performed DNS of a single orifice resonator with high-speed grazing flow. It was observed that the vortex shedding behavior changes with the incident acoustic wave frequency, with lower frequencies leading to more intense vortex shedding. The results showed that the higher the grazing flow Mach number, the less the shed vortices were able to advect towards outer regions of the boundary layer, which could impact the performance of neighboring resonators. Tam et al. [7] carried out experiments in the NASA Langley Grazing Flow Impedance Tube (GFIT) to provide experimental reference data to validate numerical results of a row of eight slit resonators. The impedance mismatch, found at lower frequencies, was attributed to reflections at the terminations of the experimental setup. Furthermore, the study discovered that the liner generates self-noise via a feedback loop mechanism at relatively high frequencies. The same experimental data has been used by Zhang and Bodony [8], who performed DNS of a single cavity resonator, and by Avallone et al. [9], who considered a multi-orifice resonator with a lattice-Boltzmann (LB) based solver, both accounting for the presence of grazing flow. These works provide a deep look into the flow-acoustic interactions and their effects. Good agreement on the impedance results were achieved. However, both studies were limited to a single cavity, thus preventing the investigation of cavity-cavity interactions and comparison with experimental data from impedance eduction techniques.

The need to investigate multi-cavity liners comes from recent works, where differences in measured impedance were found when using different eduction methods and when changing the relative direction of propagation of the acoustic wave with respect to the main flow. The latter was first reported by Renou and Aurégan [10], who attributed the mismatch to a failure of the Ingard-Myers [11, 12] boundary condition (BC), which is typically applied in the acoustic propagation models used by eduction methods. A large comparison with experimental data from different facilities and eduction methods has shown that the mismatch between liner's impedance educed considering upstream and downstream propagation is not an artifact [13]. Since then, different boundary conditions have been proposed to represent the liner in the presence of a sheared flow [14, 15], and as discussed by Spillere et al. [16], none was found to be truly predictive. Thus, the investigation towards physically accurate boundary conditions for acoustic liners in the presence of flow remains an open topic.

Recently, a realistic multi-cavity SDOF liner was simulated by Schroeder et al. [17] through a LB solver. They analyzed the same liner experimentally investigated by Spillere et al. [18]. Simulations were performed without grazing flow and the impedance was obtained with both the in-situ [19] and the mode matching method [20]. Simulations results showed good agreement with experimental data.

In this paper, we present a follow-up of the work presented by Schroeder et al. [17], where the same multi-cavity SDOF liner is investigated in the presence of flow, and the comparison between eduction methods is extended by including the Prony-like Kumaresan-Tufts (KT) technique [21]. Numerical results are presented for acoustic plane wave with tonal frequency equal to 800, 1100, 1400, 1700, 2000 and 2300 Hz (i.e., above and below the resonant frequency) and amplitude equal to 130 dB and 145 dB. Both the no-flow ($M = 0$) and grazing turbulent flow cases ($M = 0.3$) are investigated. The numerical results are compared to experimental data obtained in the UFSC impedance test rig, where synchronous microphone measurements were carried out to educe impedance with the three different approaches (in-situ technique, mode matching method and KT algorithm).

This paper is structured as follows. Section II provides a description of simulation setup and the numerical method. Section III describes the impedance measurement techniques applied to both experimental and numerical results. Section IV presents the acoustic numerical results, which are compared to experimental data. The experimental and numerical flow profiles are presented and compared, and the effects of the grazing flow and the relative direction of the acoustic source on the liner's impedance are analyzed. Section V provides the main conclusions of the paper.

II. Numerical Method and Computational Setup

A. Lattice-Boltzmann Method

The lattice-Boltzmann method (LBM) has been widely used to address fluid dynamic problems in the past years. Recently, it has been used to investigate different aeroacoustic problems [22–24]. Detailed descriptions of the theory involving the LBM can be found in several texts [25–27].

The Boltzmann equation, which is based on the kinetic theory of gases, is the starting point of the LBM derivation. It models the fluid in a mesoscopic scale, based on the statistical description of the particles' motion in terms of the particle distribution function $f(\mathbf{x}, \xi, t)$, which represents the probability of finding particles with velocity ξ at a certain position $\mathbf{x}$ and time t. A formal relation to the macroscopic scale is achieved through a scale expansion technique, known as Chapman-Enskog [28].

Numerically, the continuous velocity space is discretized by Hermite orthogonal polynomials expansion into a finite number of directions so as to provide the space-discrete distribution function $f_i(\mathbf{x}, t)$, where the subindex i denotes a discrete velocity direction [27]. The distribution of particles is stored in a Cartesian mesh, known as lattice, and each component i of a distribution function is advected from one node of the computational lattice to the neighboring ones during a single time step. Every time step consists of two essential operations: streaming and collision. In the streaming operation, the f_i functions are forced to advect from one lattice element to an adjacent one. In the collision operation, a local thermodynamic equilibrium state is set for each of the discrete directions, by means of energy exchange between particles.

In this work, the numerical simulations are performed with the commercial LB solver 3DS-Simulia PowerFLOW 6-2021-R2 [29]. The discrete LB equations are solved for 19 symmetrical directions in a 3D space (D3Q19). Any solid surface within the lattice is discretized, and the interaction between a fluid particle and a surface element can be dictated by two boundary conditions: the free-slip and the no-slip. The free-slip boundary condition enforces only zero normal fluid velocity on the surface to which it is applied, while placing no restrictions on the tangential fluid velocity. The no-slip boundary condition enforces both zero normal fluid velocity and zero tangential fluid velocity. Periodic boundary condition is applied to the borders of the simulation domain which are not delimited by any solid surface. This BC conserves mass and momentum [25].

Because of the high Reynolds number for the case of interest, a Very Large Eddy Simulation approach is adopted, where only the large turbulent scales are resolved, while the smaller scales are modelled [30]. The numerical scheme uses a turbulence model that consists of a modification of the two-equation Renormalization Group Theory (RNG) $k - \varepsilon$ [31, 32], which adjusts the Boltzmann model to the characteristic turbulent time scale.

The software applies a wall model based on the law-of-the-wall [32].

B. Liner Geometry and Computational Domain

In this study, the same liner geometry and computational approach presented by Schroeder et al. [17] are considered. As shown in Fig. 1, the geometry consists of a SDOF liner with eleven square cavities of width l = 9.20 mm separated by walls of thickness w = 0.80 mm, resulting in a streamwise sample length of L = 110 mm. The face sheet of thickness τ = 0.80 mm has 6 orifices of diameter d = 1.00 mm per cavity, which gives a percentage of open area (POA) of 5.6%. The cavities are h = 38.50 mm high and are completely separated from each other.
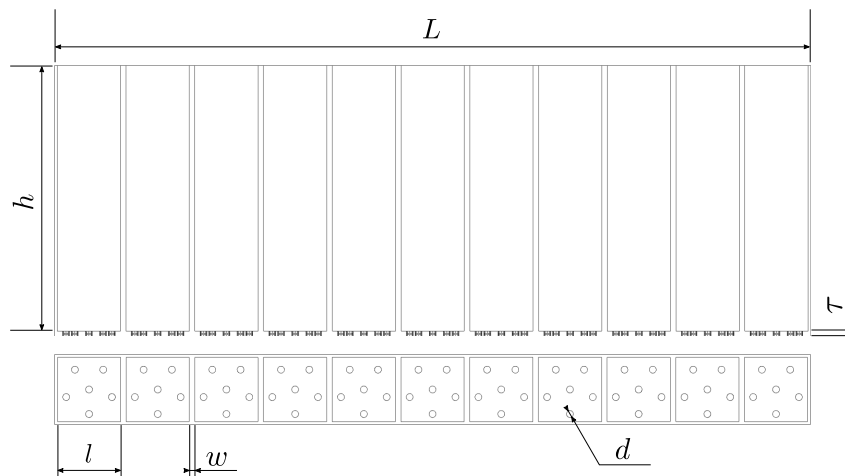

Fig. 1 Modelled liner row geometry.

Fig. 2 presents the numerical domain used in this study. The coordinate system is placed in the midsection of the liner sample. The x axis is oriented in the streamwise direction. The UFSC test rig has a rectangular cross section that

3

is $2H$ = 40 mm high (y direction) and $2W$ = 100 mm wide (z direction), which corresponds to a cutoff frequency for plane wave propagation at 3400 Hz [16]. The simulation domain is H = 20 mm high, with a free-slip condition applied to the wall opposite to the sample, and 10 mm wide with a periodic BC in the z direction.

Taking Fig. 2 as reference, the duct's inlet and outlet are represented by the orange rectangles. At the inlet, pressure and velocity BC are set, while a pressure BC is set at the outlet. The purple color represents sponge regions set at the duct's terminations, where the fluid's viscosity is increased to prevent reflections of acoustic waves. The absorbing region is 3λ long, where λ corresponds to the largest wavelength considered in this set of simulations. Free-slip BC is applied to the gray colored walls, and the blue colored ones are set as no-slip. The VLES algorithm is triggered to solve the turbulent scales next to the top wall. This is done by placing a tripping geometry upstream of the liner, as detailed in Fig. 2. The resolution in the liner's orifices is used as reference for the lattice refinement scheme. The grid refinement becomes coarser towards the center and the ducts' terminations to reduce the computational cost. In the rest of the work results for a resolution of 25 cells per orifice diameter resolution are presented, together with some higher resolution results (50 cells per orifice) for specific cases.
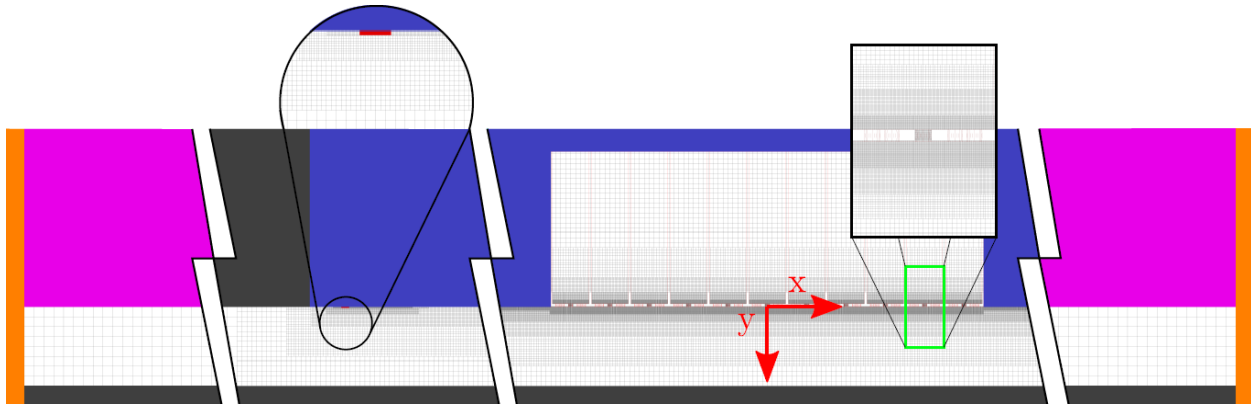

Fig. 2   Simulation domain: lattice representation and reference coordinate system.

The acoustic simulations are performed by superimposing a harmonic acoustic plane wave to the fluid domain by using the *Opty∂B* toolkit [33]. The velocity field time convergence is assessed by the evaluation of the time history of the boundary layer thickness δ, the friction velocity u_τ and the maximum Mach number M. It is considered that the flow velocity field has converged after a relative deviation within a 1% range is verified for all parameters simultaneously. Acoustic simulations are conducted for 800, 1100, 1400, 1700, 2000 and 2300 Hz at 130 and 145 dB, both without and with turbulent grazing flow at maximum Mach number of M = 0.3, and with the acoustic source located both at upstream and downstream positions relative to the liner sample.

C. Velocity Field Validation

The comparison between the experimental velocity field and the numerical one is performed by comparing the x component of the flow velocity U at the upstream end of the liner sample, as indicated in Fig. 3. To measure the flow experimentally, the liner sample is replaced by a custom apparatus which contains a Pitot tube. The flow velocity data is gathered in a set of y positions in the central z section of the duct.

The analytical model presented by Schlichting and Gersten [34] is used for the turbulent boundary layer (TBL) characterization, through a numerical least-square fitting procedure over both the experimental and simulation's data. The flow profile definition relies on the adjustment of two parameters: the friction velocity u_τ and the boundary layer thickness δ. It is worth mentioning that δ is very difficult to determine, thus it is often approximated by δ_{99}, i.e., the y coordinate in which $U(y) \approx 0.99U_\infty$, being U_∞ the free-stream velocity.
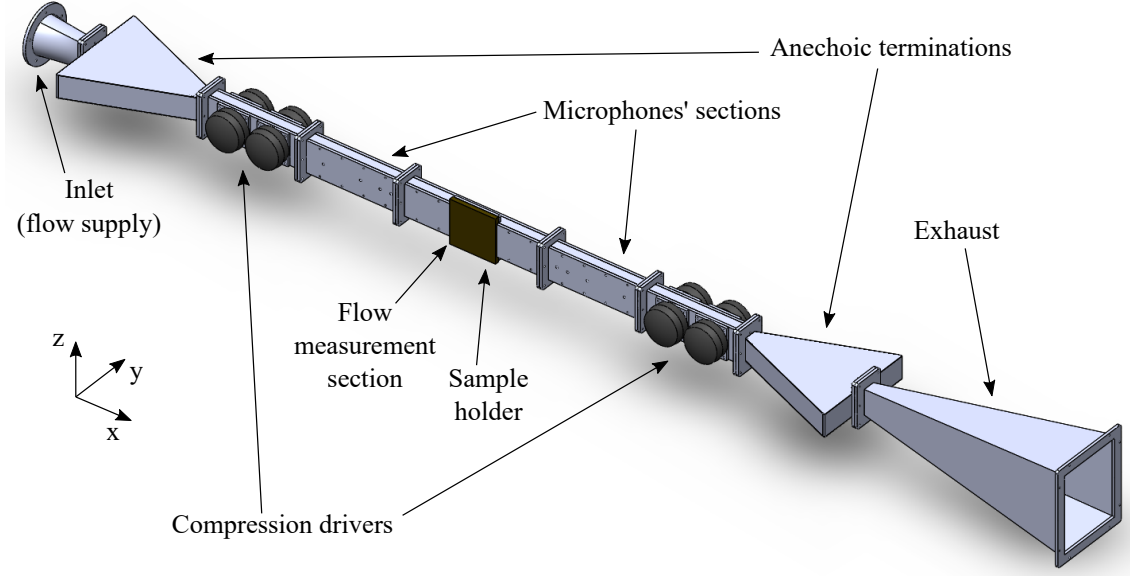
4

Fig. 3   Representation of the UFSC experimental setup.

Taking the coordinate system of Fig. 2 as reference, the flow profile is defined by

$$u^+ = y^+, \qquad\qquad y^+ < 5, \quad (1a)$$

$$u^+ = \frac{1}{\Lambda}\left[\frac{1}{3}\ln\frac{\Lambda y^+ + 1}{\sqrt{(\Lambda y^+)^2 - \Lambda y^+ + 1}} + \frac{1}{\sqrt{3}}\left(\tan^{-1}\frac{2\Lambda y^+ - 1}{\sqrt{3}} + \frac{\pi}{6}\right)\right] + \frac{1}{4\kappa}\ln\left(1 + \kappa B y^{+4}\right), \quad 5 < y^+ < 70, \quad (1b)$$

$$u^+ = \frac{1}{\kappa}\ln y^+ + C^+, \qquad\qquad y^+ > 70. \quad (1c)$$

The flow variables indicated by the superscript '+' refer to the dimensionless scale of the inner boundary layer. In Eq. 1, $y^+ = yu_\tau/\nu$, where ν is the fluid's kinematic viscosity. Similarly, U relates to u^+ by $u^+ = U/u_\tau$. The other parameters are the von Kármán constant $\kappa = 0.41$, $A = 6.1 \times 10^{-4}$, $B = 1.43 \times 10^{-3}$ and $\Lambda = (A + B)^{1/3}$, which gives $C^+ = 5$. These parameters were defined by extensive numerical evaluations and experimental measurements [34].

III. Impedance Measurement Techniques

A. In-Situ Technique

The in-situ technique, developed by Dean [19], is the simplest method to assess the liner's impedance. It relies on the acquisition of the acoustic pressure at the face sheet $\tilde{P}_f$ and at the back plate $\tilde{P}_b$, as shown in Fig. 4. The transfer function between these complex acoustic pressures can be obtained as $\tilde{H}_{pair} = \tilde{P}_f/\tilde{P}_b$. The local liner impedance $\tilde{Z}_c$ is then determined by

$$\tilde{Z}_c = -\mathrm{i}\tilde{H}_{pair}\frac{1}{sin(\zeta h)}, \qquad (2)$$

where $\mathrm{i} = \sqrt{-1}$, h is the cavity height, and $\zeta = \omega/c$ is the free-field wavenumber, with ω the acoustic wave angular frequency and c the sound speed.

The implementation of this technique in LBM has already been proven effective and capable of delivering good results [9]. A recent study has shown that, in the absence of grazing flow, the resistance and SPL tend to decrease along the liner's length, as the acoustic wave interacts with successive cavities in a row, and this behavior is more noticeable near the resonant frequency [17]. Meanwhile, the reactance tends to increase along the liner's length [17].
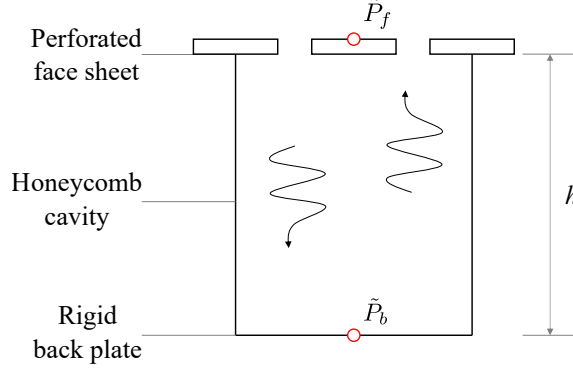
5

Fig. 4   In-situ technique schematic: pressure probing locations.

Because of this behavior, the impedance $\tilde{Z}_c$ obtained for one cavity might not be representative for the whole sample. Experimentally, it is not common nor practical to sample all cavities, and the results presented in this work are obtained for the cavity nearest to the acoustic source. Numerically, it is possible to sample all cavities, and in this case the results presented here are in the form of a mean value among all cavities.

B. Mode Matching Method

The mode matching (MM) method is a inverse impedance eduction technique that relies in a model of the acoustic field inside the duct based on the mode matching approach. The procedure adopted here is the same described in Spillere et al. [16], and a brief description is provided below.

A theoretical acoustic field $\tilde{P}_{\text{num},q}$ is calculated with the amplitudes of the plane acoustic waves propagating towards the liner sample and with an initial guess for the impedance. In order to improve convergence, semi-empirical impedance models (e.g. Murray and Astley [2]) are commonly employed as initial guess for the liner's impedance. The Levenberg–Marquadt algorithm [35, 36] is used to minimize the cost function

$$\mathcal{F}(\tilde{Z}, \omega) = \sum_{q=1}^{8} \left| \frac{\tilde{P}_{\text{exp},q} - \tilde{P}_{\text{num},q}(\tilde{Z}, \omega)}{\tilde{P}_{\text{exp},q}} \right|, \tag{3}$$

where $\tilde{P}_{\text{exp},q}$ and $\tilde{P}_{\text{num},q}$ are the experimental and numerical acoustic pressure at each microphone location x_q, leading to the liner's educed impedance. Two sets of 4 flush-mounted microphones placed upstream and downstream of the liner are used, and the red dots in Fig. 5 represent the microphones' locations.

Sound wave amplitudes $A_i^{\pm}$ are needed as input to calculate the theoretical acoustic field, which are also obtained from the acoustic pressure measured by the microphones. The amplitudes are obtained by an over-determined plane wave decomposition procedure. For example, in the upstream section

$$\begin{bmatrix} \exp(-i\zeta_{x,1}^{+}x_1) & \exp(-i\zeta_{x,1}^{-}x_1) \\ \exp(-i\zeta_{x,1}^{+}x_2) & \exp(-i\zeta_{x,1}^{-}x_2) \\ \exp(-i\zeta_{x,1}^{+}x_3) & \exp(-i\zeta_{x,1}^{-}x_3) \\ \exp(-i\zeta_{x,1}^{+}x_4) & \exp(-i\zeta_{x,1}^{-}x_4) \end{bmatrix} \begin{bmatrix} A_1^{+} \\ A_1^{-} \end{bmatrix} = \begin{bmatrix} \tilde{P}_{\text{exp},1} \\ \tilde{P}_{\text{exp},2} \\ \tilde{P}_{\text{exp},3} \\ \tilde{P}_{\text{exp},4} \end{bmatrix}, \tag{4}$$

and similarly for the downstream section. In Eq. 4, the superscripts '+' and '-' refer to the direction of propagation of the acoustic wave components, which are the downstream and upstream directions, respectively. The microphones' streamwise positions are represented by x_i. The plane wave axial wavenumber $\zeta_{x,1}^{\pm} = \pm\zeta K_0/(1 \pm K_0 M)$ also accounts for viscothermal losses at the duct walls given by the first order Kirchhoff solution K_0 [37].

C. The Prony-like Kumaresan-Tufts (KT) Algorithm

Impedance eduction based on Prony method was first proposed by Jing et al. [38]. In this case, the microphones are flush-mounted at the wall opposite to the liner sample, as schematically shown by the blue dots in Fig. 5. The

6

method is based on the assumption that the acoustic field at the lined section is a linear combination of damped complex exponentials, giving

$$\tilde{P}_i(x) = \sum_{n=1}^{\infty} A_n^{\pm} V_{n,i}, \quad i = 0, 1, ..., \mathcal{M} - 1, \tag{5}$$

where $\tilde{P}_i$ is the pressure at the i-th microphone, $V_{n,i} = \exp(-i\zeta_{x,n}^{\pm} i \Delta_x)$ contains the desired axial wavenumbers, Δ_x is the distance between two consecutive microphones and $\mathcal{M}$ is the number of microphones. In this work, the KT algorithm is used to extract the wavenumber from a set of 12 equally spaced pressure probes with $\Delta_x = 10$ mm, as described with further details in Bonomo et al. [21].
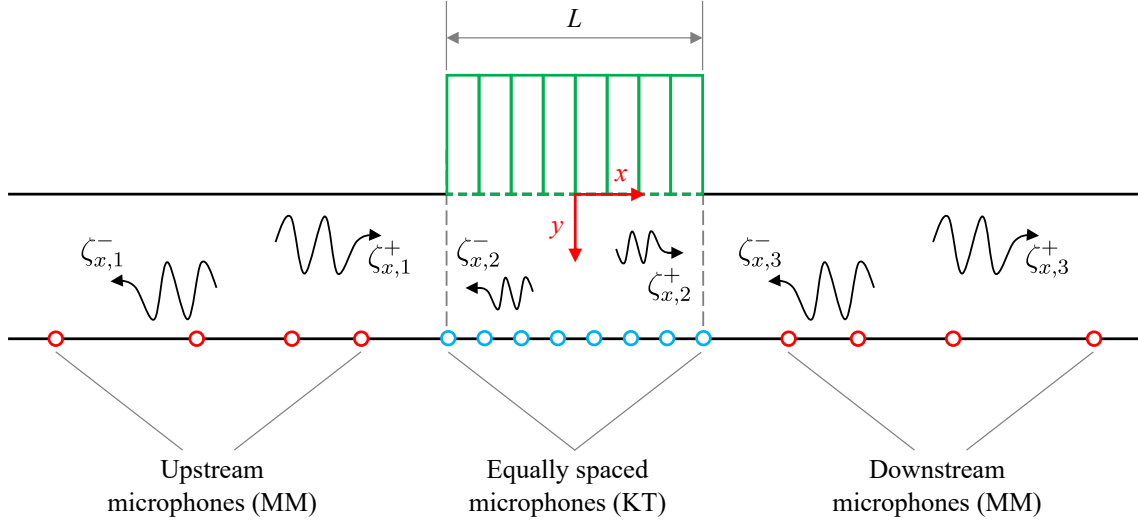

Fig. 5   Impedance eduction techniques schematic: microphones' positions.

IV. Results

The numerical acoustic results are presented and compared to the experimental ones in this section. The in-situ technique, the mode matching method and the Prony-like KT algorithm are applied to assess the liner's acoustic impedance for 800, 1100, 1400, 1700, 2000 and 2300 Hz at 130 dB and 145 dB. For the no-flow case, only an upstream acoustic source is considered, since a change in the impedance is not expected to happen in this scenario with different relative positions with respect to the liner [15]. For the case accounting for the $M = 0.3$ grazing flow, simulations for both upstream and downstream acoustic sources are performed.

A. Acoustic Results: No-Flow Cases

The comparisons of the two components of impedance from both the numerical and experimental database for the no-flow case are reported in Fig. 6. A very good agreement can be observed between numerical and experimental results, with resistance values approximately constant and equal to zero in the entire frequency range analyzed. With respect to the comparison between the three methods, while the resistance does not show any relevant difference, the reactance shows a difference between direct and inverse eduction methods. The former predicts a higher reactance below the resonance liner frequency and a lower one at higher frequency. This is observed in both the numerical and experimental results.

Increasing the amplitude of the grazing acoustic wave to 145 dB (Figs. 6c and 6d) also leads to an increase in the resistance as expected, due to the liner non-linear behavior [8], while minor variations are found for the reactance. Some differences in the resistance between experimental methods can be observed for the case with 145 dB, which is not very clear in the numerical results. The mismatch might be due to the relative low resolution of the simulations and to the adoption of a more dissipative solver, as it will be explained later. Further analysis is required in this case. From the experiments, it is found that the highest resistance is measured by the in-situ technique, while the lowest resistance is measured by the mode matching method. Furthermore, the in-situ technique shows a weak increase of the resistance

7

with increasing the frequency, while an opposite behavior is found for the mode matching results. The Prony-like KT method shows a pretty constant value of the resistance with a spike slightly below the resonance frequency, maybe caused by experimental uncertainty. An increase in resistance can be seen in the experimental mode matching results in the low-frequency range, which is attributed to uncertainties due to the small sample length compared to the acoustic wavelength, and to small attenuation levels [18]. The mode matching numerical results are in agreement with the method's experimental curve, and exhibit a similar increase in lower frequencies. The numerical KT results agree better with the mode matching experimental curve, and underestimate the experimental KT values. The numerical in-situ results do not overestimate the resistance with respect to the numerical eduction ones, as it occurs with the experimental values. This behavior can be explained by the fact that the numerical in-situ results are averaged over all cavities. It is worth mentioning that, in the experiments, results from the in-situ technique are obtained for the most upstream cavity. For such a configuration, local resistance decreases as reactance increases at downstream cavities [17]. Since the numerical results are averaged over all cavities, this could affect the numerical results' agreement to the experimental ones.

The liner's attenuation has been associated to the inflow and outflow through the cavities' orifices [5, 8]. It has been suggested that the periodic oscillation of the flow within the orifices induced by the acoustic wave dissipate the acoustic energy by viscous effects, caused by the shear layers close to the walls, and by conversion of the acoustic energy into rotational kinetic energy, in the form of vortex shedding [5]. In this sense, the flow within the orifices is a key phenomenon to analyze. The y component of the flow velocity v is plotted in Fig. 7 for the inflow and outflow cycles for the case of 2000 Hz and 145 dB. In the figure, v is normalized by c. For the no-flow case, v can be interpreted as the acoustic particle velocity. The cavities represented in Fig.7 are the closest to the acoustic source (cavity No.1) and furthest (cavity No.11). It is shown that the acoustic-induced velocity within the cavity decreases at more downstream cavities, in line with a reduction of the SPL of the grazing acoustic wave.

Fig.8 shows the change in impedance and SPL over the liner's cavities. It is noticeable that resistance values drops from cavity No.1 towards cavity No.11, while reactance tends to slightly increase. The cavities attenuation is observed by the drop in the SPL. These trends had already been verified by Schroeder et al. [17], and are confirmed in this work. This corroborates the hypothesis of the underestimation of the numerical resistance and of overestimation of the numerical reactance obtained by the in-situ technique for 145 dB.

B. Assessment and Analysis of the Turbulent Boundary Layer

For the assessment of the numerical turbulent boundary layer against the experimental one, the velocity profiles upstream of the liner at $x = -55$ mm are compared. The zig-zag trip is positioned at $x = -729$ mm. Fig. 9 shows the comparison between velocity profiles, as well as the fitting of the analytical model by Schlichting and Gersten [34]. The maximum Mach number is $M \approx 0.3$ on both the experimental and numerical profiles. Deviations can be seen between the two in the outer regions of the TBL. The numerical TBL has a thickness of $\delta_{99} \approx 7.6$ mm, while the experimental one is $\delta_{99} \approx 11.2$ mm thick. Since the experimental curve was sampled by a Pitot tube, it lacks information of the inner region of the TBL. The friction velocity is obtained by the theoretical fit for both cases for the sake of comparison. It is found that $u_\tau \approx 4.30$ m/s for the numerical case and $u_\tau \approx 4.13$ m/s for the experimental one. Differences are found also also in terms of integral boundary layer parameters, such as the displacement thickness δ^* and the momentum thickness θ. In the following, they are normalized with respect to the diameter of the orifice d. For the numerical profile $\delta^*/d \approx 0.73$ and $\theta/d \approx 0.60$, while for the experimental $\delta^*/d \approx 1.02$ and $\theta/d \approx 0.83$. The interaction between the turbulent flow and the orifice is strongly dependent on the integral TBL parameters [9]. As a baseline, Zhang and Bodony [8] worked with about 5% deviation between experimental and numerical δ^* and less than 2% deviation for θ. In this work, almost 40% of deviation can be found for both δ^*/d and θ/d, which could affect the correlation between experimental and numerical acoustic results. Further improvements of the flow will be needed in the future.

The turbulent flow interaction with the orifice leads to the formation of a circulation regions inside the orifice, which affects the interaction of the acoustic wave with the liner [5, 9]. A time-averaged flow-field is represented in Fig. 10 for a streamwise slice at $z = 0$. The figure shows the contour plot of v, the streamlines of the flow inside the cavities and the flow velocity vectors near the orifice. Specifically for this figure, the y axis positive direction is reversed with respect to the coordinate system established in Fig. 2. A counter clockwise circulation region appears inside the orifices, which forces the development of a clockwise flow circulation in the mid-region of the cavities' height. Minor circulation regions also appear near the orifices next to the cavities' upstream divisions, which exhibit counter clockwise rotation, and deep inside the cavity, whose behavior is rather random. These findings agree with those in Tam et al. [5] and Avallone et al. [9].
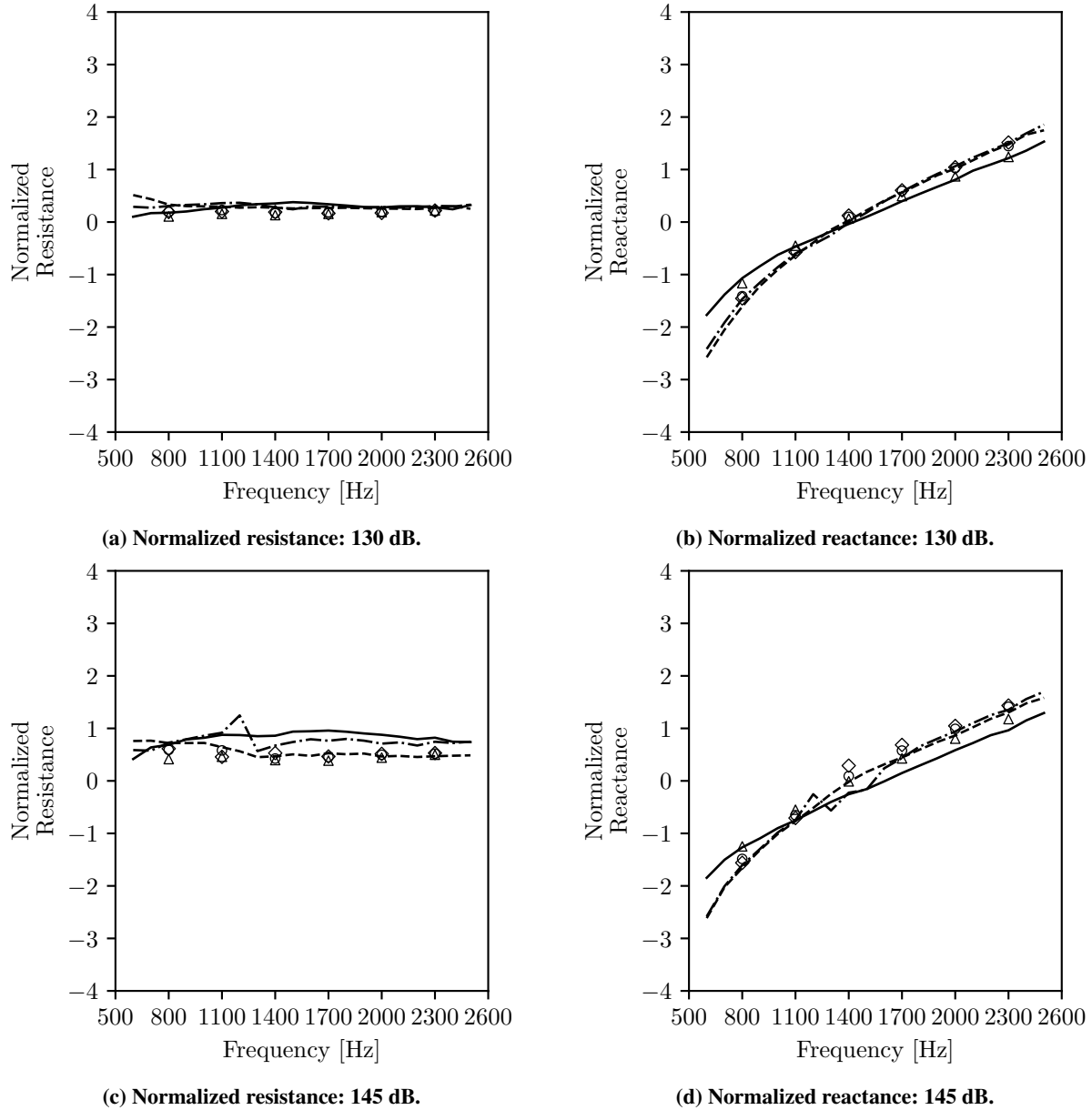
(a) Normalized resistance: 130 dB.

(b) Normalized reactance: 130 dB.

(c) Normalized resistance: 145 dB.

(d) Normalized reactance: 145 dB.

Fig. 6   Normalized impedance for the no-flow case as a function of the incident acoustic wave frequency: (—) experimental [in-situ]; (- -) experimental [MM]; (-·-) experimental [KT]; (△) numerical [in-situ]; (○) numerical [MM]; (◇) numerical [KT].

The presence of the vortex inside the orifice can be responsible for an increase in the liner's resistance due to the smaller effective area of the orifice where the oscillation induced by incident acoustic wave takes place [33]. This vortex is said to be quasi-steady, because it slightly oscillates within the orifice [33]. It is of primary importance to get a good representation of the fluid dynamics in this region of the model, which include the quasi-steady vortex dimensions and its interaction with the acoustic perturbations.

C. Acoustic Results: Grazing Flow Cases
Results for the case with the acoustic wave propagating in the same direction of the mean flow are shown in Fig. 11. For the 130 dB case, normalized resistance and reactance are presented in Figs. 11a and 11b, respectively, while
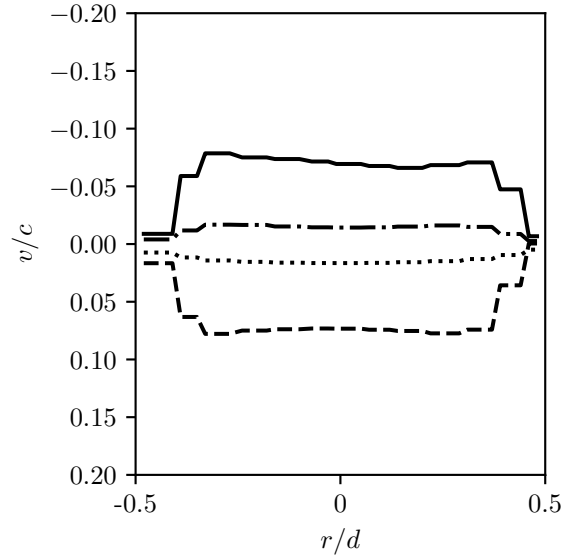
9

Fig. 7   Velocity profile inside the central orifice of the cavities at $z = 0$**: (—) cavity No.1 [inflow]; (- -) cavity No.1 [outflow]; (-·-) cavity No.11 [inflow]; (····) cavity No.11 [outflow]. Data for the 2000 Hz at 145 dB case, with** $M = 0$**.**
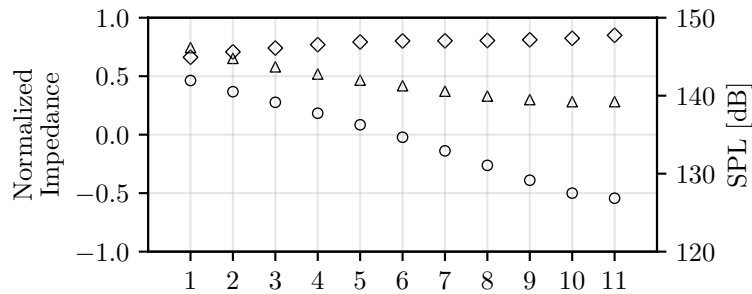

Fig. 8   Normalized impedance and SPL calculated at each of the liner's cavities: ($\triangle$) **resistance;** ($\diamond$) **reactance;** ($\bigcirc$) **SPL. Data for the 2000 Hz at 145 dB case with** $M = 0$**.**

Figs. 11c and 11d refer to the 145 dB case. The experimental results exhibit significantly higher value for the resistance when compared to the no-flow case results, which is expected due to the effects of the grazing flow [10, 18, 39]. In this scenario, the grazing flow non-linear effects dominate the non-linear effects due to the increase in SPL, and there is no significant difference between the experimental values obtained for 130 dB and 145 dB. The behavior of the curves for the three methods with respect to each other are consistent with what is observed in the no-flow case results. The in-situ technique tends to underestimate the resistance measured with the eduction methods in the lower frequency range, while it overestimates them at higher frequencies. Good agreement among methods is seen in the mid-frequency range. Reactance results exhibit minor changes, when compared to the no-flow case. The eduction methods still agree at higher frequencies, but show a mismatch at lower frequencies. The in-situ results show a different trend from what is observed in the no-flow case, this time overestimating with respect to the eduction methods at all frequencies.

In general, the numerical results show similar trends, but they considerably overestimate the experimental values by approximately a factor of 2. The numerical results for the reactance are closer to the experimental baseline, exhibiting minor changes with respect to the no-flow case. Still, there is significant discrepancy between the different methods' results, and an outlier can be seen for the 800 Hz KT result at 130 dB.

Considering the downstream acoustic source, results are shown in Fig. 12. Resistance and reactance are plotted in Figs. 12a and 12b, respectively, for the source at 130 dB. For the source at 145 dB, resistance and reactance are shown in Figs. 12c and 12d, respectively. In this scenario, the resistance obtained experimentally by the in-situ technique is
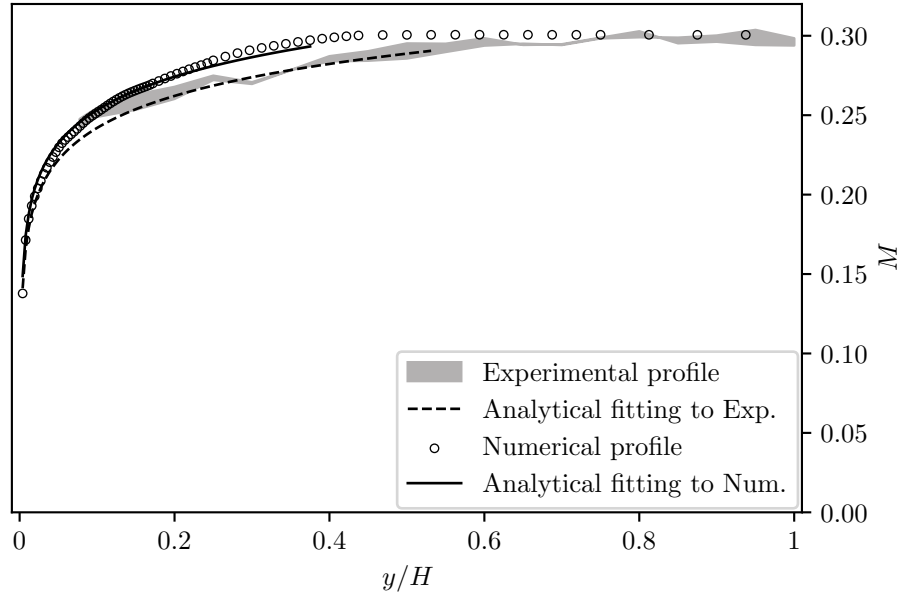
Fig. 9 Flow profile at the upstream end of the liner sample: experimental, numerical and analytical fitting as per Schlichting and Gersten [34].
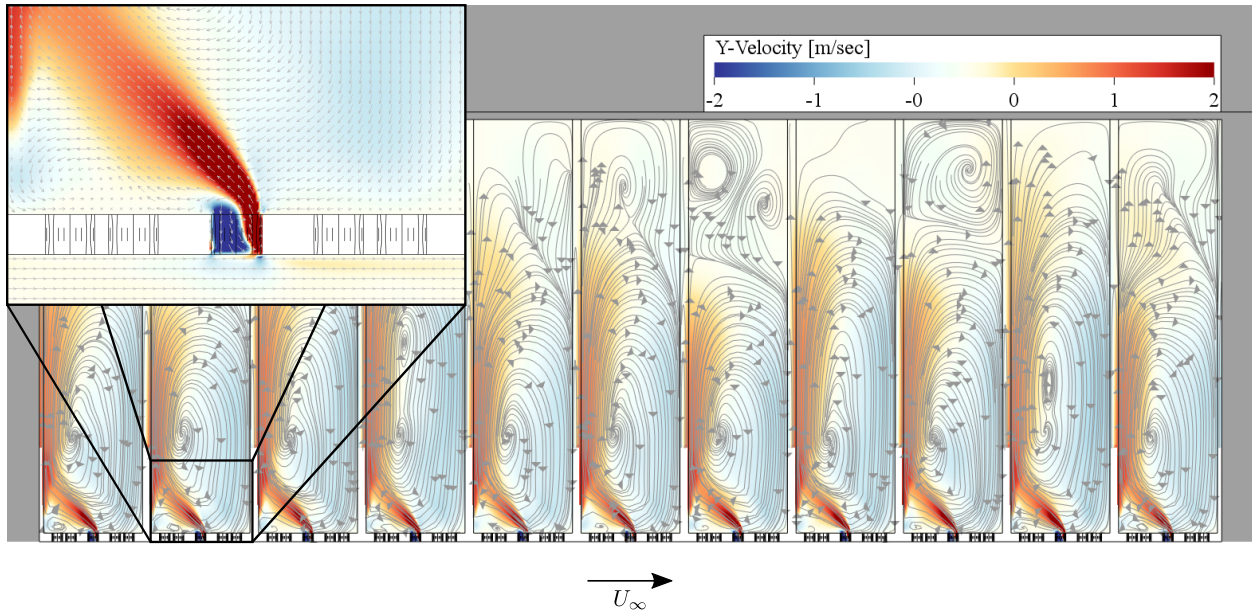

Fig. 10 Contour plot of the *y* velocity component of the flow, streamlines inside the cavities and detailed near orifice velocity vectors.

rather constant over all the frequency range for both SPLs, and it is lower than the one obtained by the eduction methods. The resistances obtained by the eduction techniques are similar. The same agreement is seen in the reactance results. The reactance obtained with the eduction methods is higher than the one obtained by the in-situ technique for both SPLs, especially at lower frequencies. The numerical results also show the increase in resistance due to the grazing flow in this case, however, the methods present great discrepancies with respect to each other. Fluctuations in the trends are present in the numerical results, particularly for the 130 dB case, where the acoustic wave signal to turbulence noise ratio is lower, and then it becomes harder to capture the acoustic effects in the time signals. A similar overestimation of the resistance from the numerical results with respect to the experimental baseline is present, as it happens for the upstream
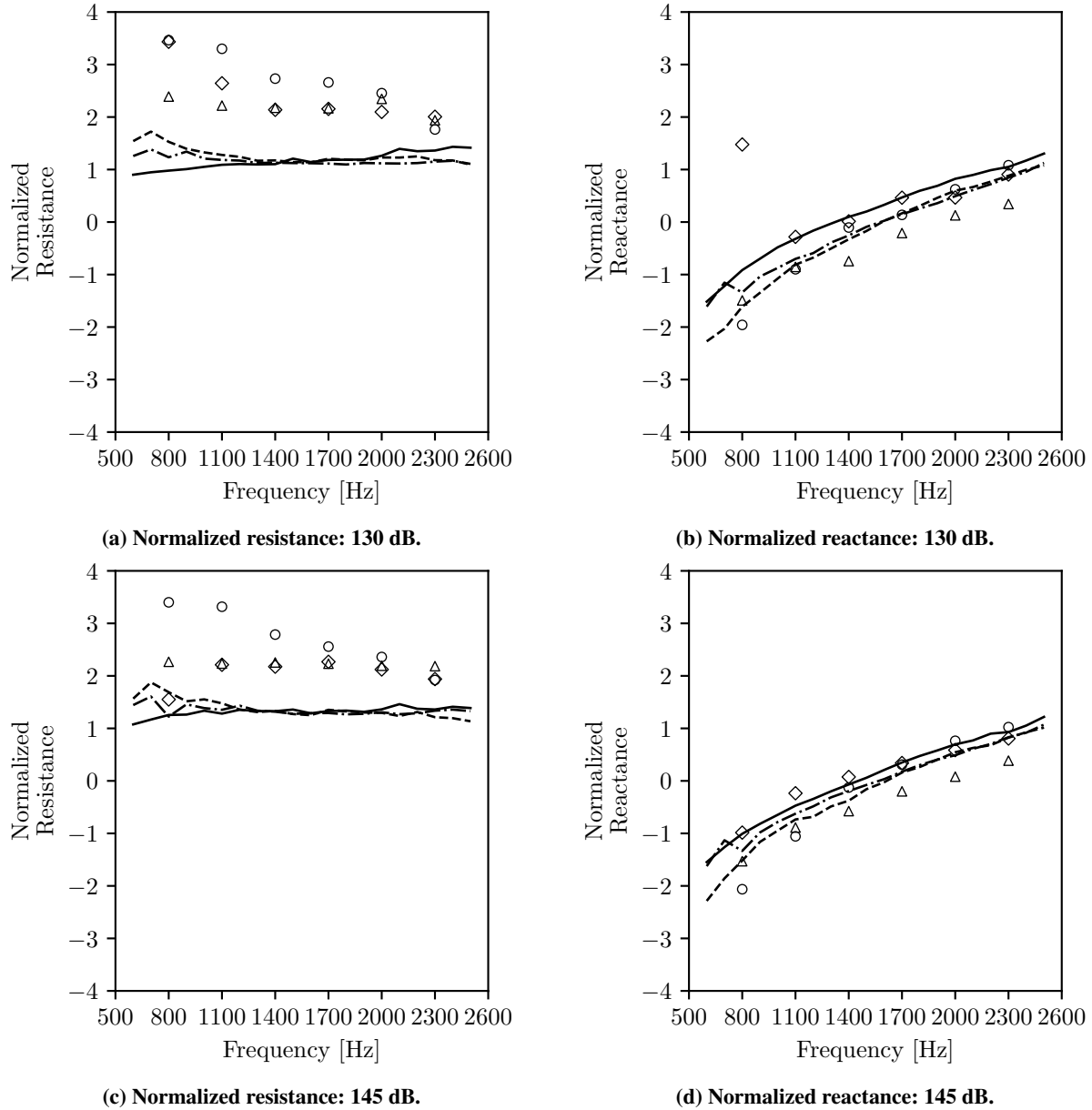
11

(a) Normalized resistance: 130 dB.

(b) Normalized reactance: 130 dB.

(c) Normalized resistance: 145 dB.

(d) Normalized reactance: 145 dB.

Fig. 11 **Normalized impedance for the** $M = 0.3$ **grazing flow case as a function of the incident acoustic wave frequency (upstream source): (—) experimental [in-situ]; (- -) experimental [MM]; (-·-) experimental [KT]; (△) numerical [in-situ]; (○) numerical [MM]; (◇) numerical [KT].**

source case. The numerical results for the reactance agree better than the resistance with the experimental curves. To address the low signal to noise ratio in the 130 dB case, either better post-processing or longer sampling time might be needed.

The comparison of each methods' results, considering acoustic sources at upstream and downstream positions relative to the liner sample, is presented in Fig. 13 for the in-situ technique, in Fig. 14 for the MM method and in Fig. 15 for the KT. All the impedance assessment methods exhibit different results for both resistance and reactance with the change in the source's position. Experimentally, the resistance measured by the in-situ technique shows a drop in the entire the frequency range when the relative position of the acoustic source changes from upstream of the sample to a downstream position. The numerical model is also sensitive to the change in the source's position, and shows approximately the same trend. The in-situ experimental results for the reactance also drop when the source changes

(a) Normalized resistance: 130 dB.

(b) Normalized reactance: 130 dB.

(c) Normalized resistance: 145 dB.

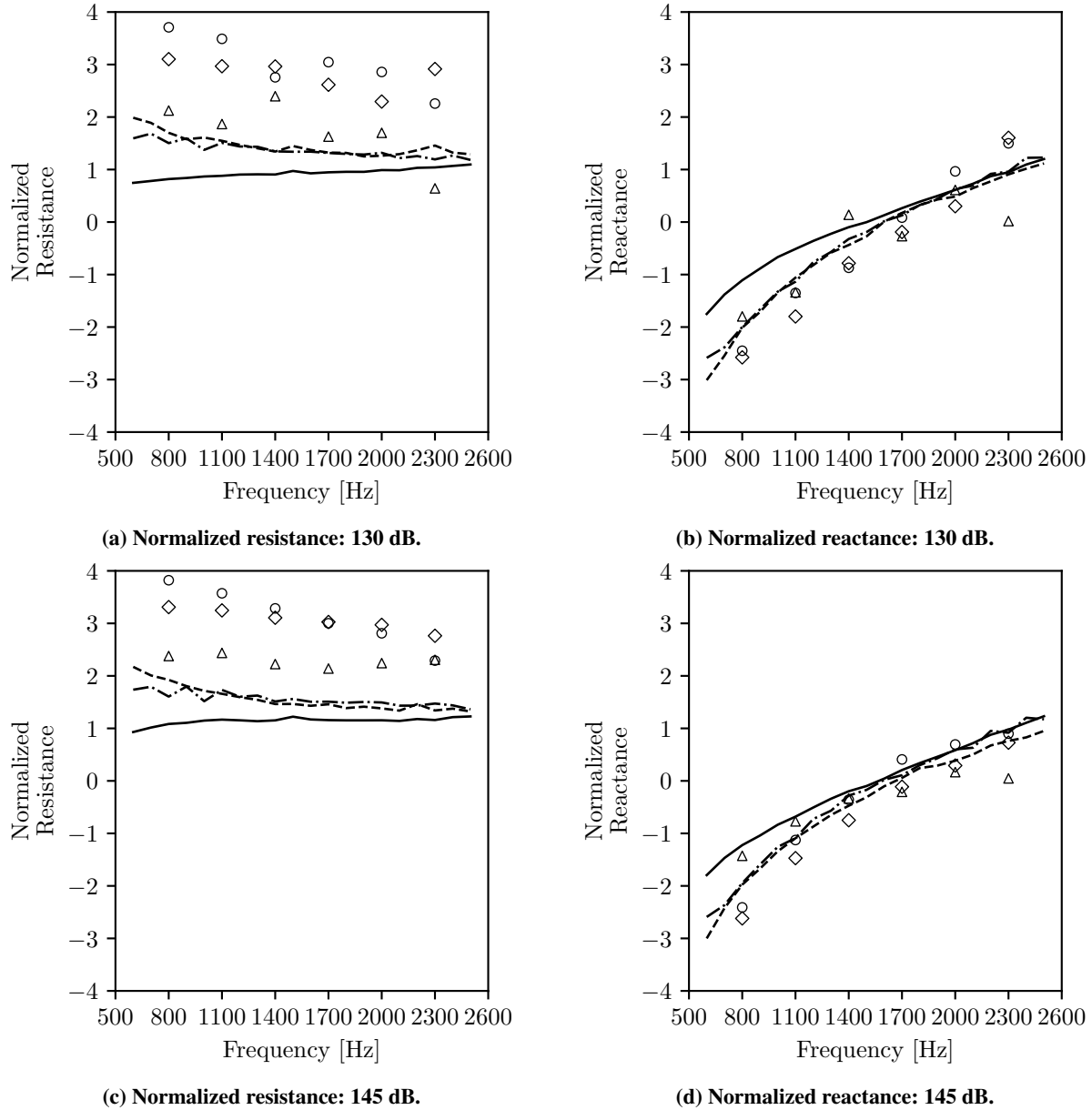**(d) Normalized reactance: 145 dB.**

Fig. 12 Normalized impedance for the $M = 0.3$ grazing flow case as a function of the incident acoustic wave frequency (downstream source): (—) experimental [in-situ]; (- -) experimental [MM]; (-·-) experimental [KT]; ($\triangle$) numerical [in-situ]; ($\bigcirc$) numerical [MM]; ($\diamondsuit$) numerical [KT].

from upstream to downstream. The numerical results represent different reactance depending on the source's position, although no pattern can be identified. These conclusions are valid for both the 130 dB and the 145 dB cases, shown in Figs. 13a and 13b, respectively.

The change in the impedance obtained by the MM method with the acoustic source positioned upstream and downstream of the liner is shown in Figs. 14a and 14b for 130 dB and 145 dB, respectively. The experimental results for the downstream source show an increased resistance with respect to the upstream values for the whole frequency range. In general, the numerical model replicates this trend for both SPLs considered. The reactance obtained experimentally drops when the source changes from an upstream position to downstream. Regarding the reactance, the numerical model also exhibits sensitivity to the source's position, although it is rather difficult to identify any pattern.

The KT algorithm is also sensitive to the acoustic source's position. The results obtained by this method are
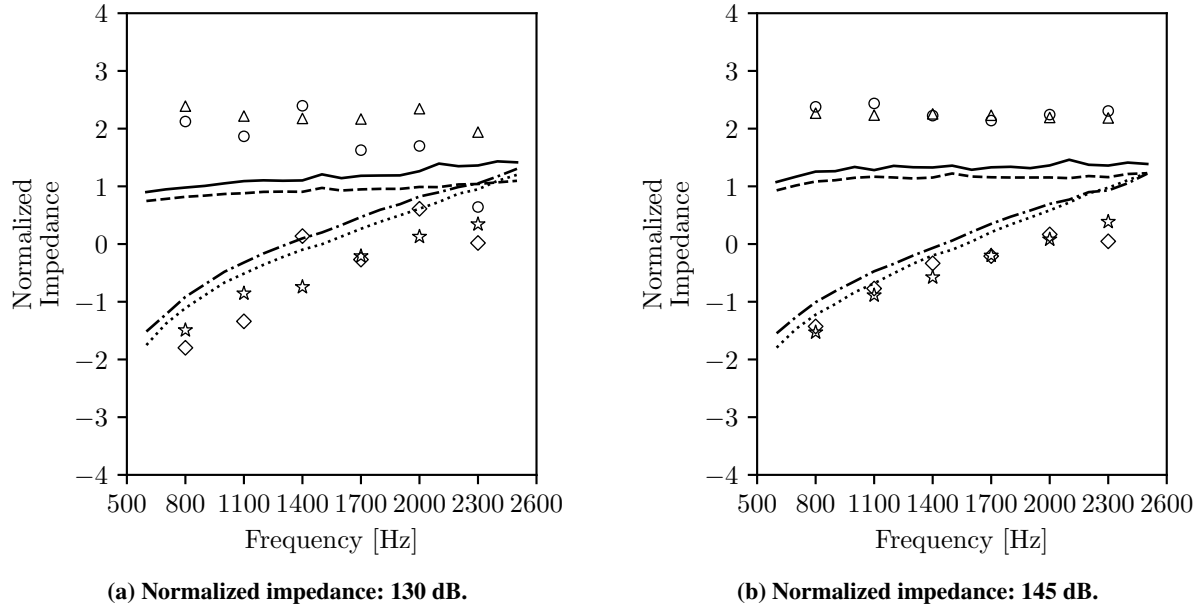
13

(a) Normalized impedance: 130 dB.

(b) Normalized impedance: 145 dB.

Fig. 13   Normalized impedance for the M = 0.3 **grazing flow case as a function of the incident acoustic wave frequency (in-situ technique). For upstream source: (—) experimental [resistance]; (- ·-) experimental [reactance]; (△) numerical [resistance]; (☆) numerical [reactance]. For downstream source: (- -) experimental [resistance]; (····) experimental [reactance]; (◯) numerical [resistance]; (◇) numerical [reactance].**

(a) Normalized impedance: 130 dB.
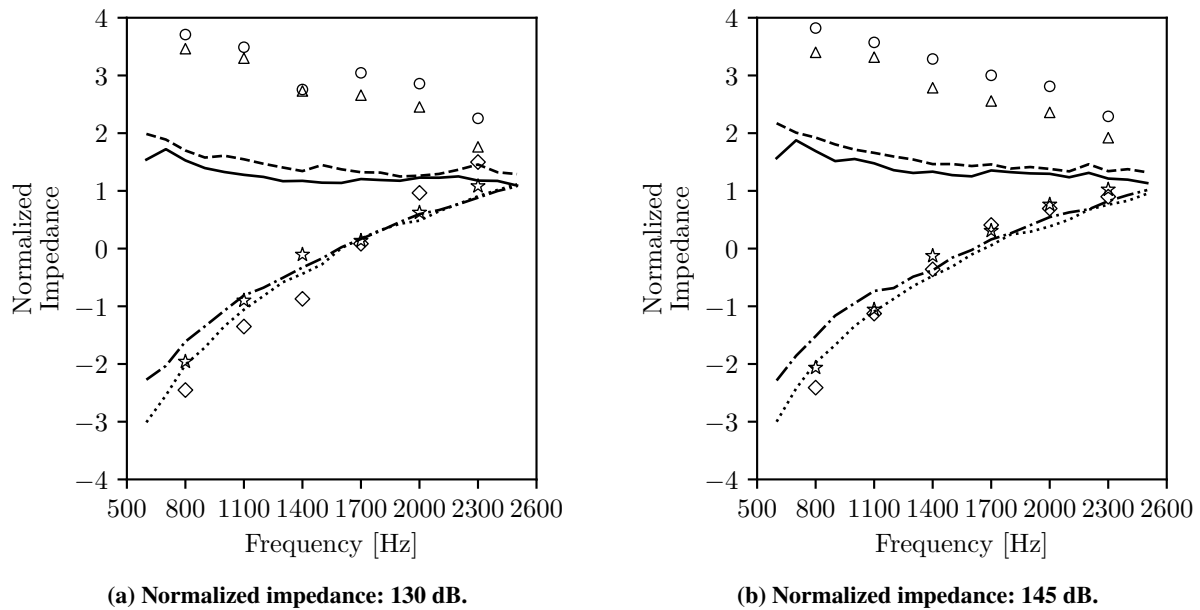
(b) Normalized impedance: 145 dB.

Fig. 14   Normalized impedance for the M = 0.3 **grazing flow case as a function of the incident acoustic wave frequency (mode matching method). For upstream source: (—) experimental [resistance]; (- ·-) experimental [reactance]; (△) numerical [resistance]; (☆) numerical [reactance]. For downstream source: (- -) experimental [resistance]; (····) experimental [reactance]; (◯) numerical [resistance]; (◇) numerical [reactance].**

shown in Figs. 15a and 15b. The analysis of the experimental results reveal a similar behavior to that exhibited by the MM method's results. An increase is seen in the resistance when the source's position changes from upstream to the

downstream of the liner. Meanwhile, reactance drops when the same change in the source's position occurs. This behavior is verified for both SPLs. It is evident that the numerical model replicates the same trends verified in the experimental baselines, with the 145 dB results showing the effects more clearly.

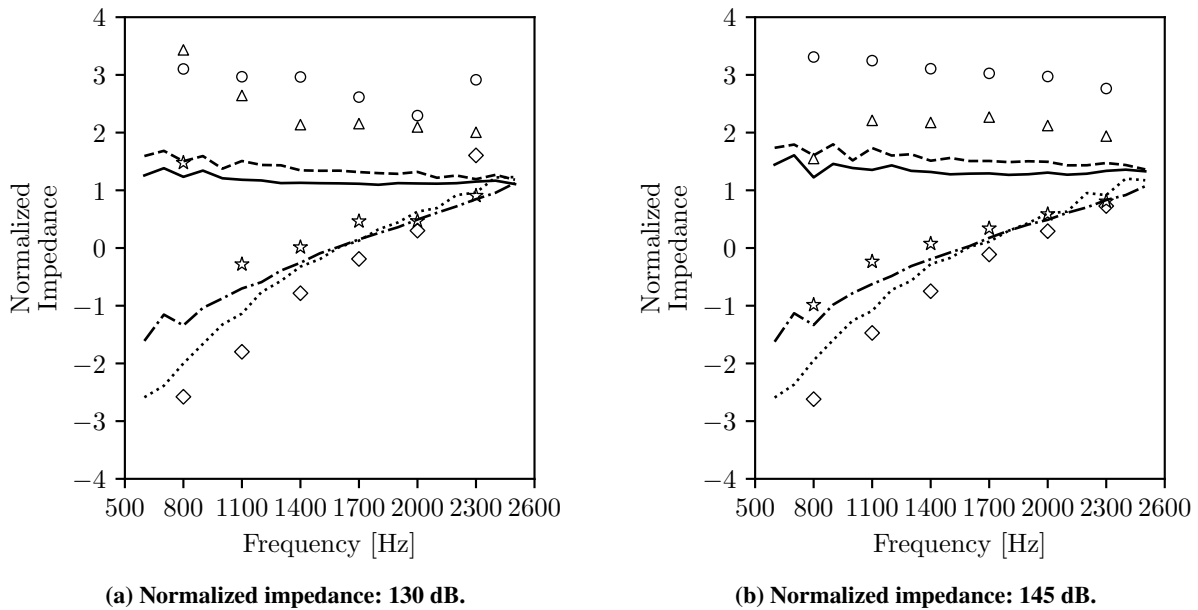**(a) Normalized impedance: 130 dB.** **(b) Normalized impedance: 145 dB.**

Fig. 15   Normalized impedance for the $M = 0.3$ grazing flow case as a function of the incident acoustic wave frequency (KT algorithm). For upstream source: (—) experimental [resistance]; (-·-) experimental [reactance]; (△) numerical [resistance]; (☆) numerical [reactance]. For downstream source: (- -) experimental [resistance]; (····) experimental [reactance]; (○) numerical [resistance]; (◇) numerical [reactance].

All methods exhibit a mismatch in the impedance assessed with the change in the acoustic source's position with respect to the liner sample, both experimentally and numerically. In general, the eduction methods predict a higher resistance when the acoustic source is at a downstream position with respect to the liner than when the source is at an upstream position. The eduction methods' predictions for the reactance are higher when the acoustic source is upstream than for the case of downstream positioned source. These findings are in agreement with previous works by Renou and Aurégan [10] and Spillere et al. [16]. Regarding the in-situ technique, an opposite behavior is observed in the resistance results. The resistance predicted by the in-situ technique is higher for the upstream positioned source with respect to the downstream positioned source. As for the reactance, the trends are similar to the eduction results, with higher values predicted for the upstream source. The works by Boden et al. [13] and Spillere et al. [18] also highlight the difference in the predicted impedance by the in-situ technique for different acoustic source's positions. The results presented by Spillere et al. [18] are in agreement with the findings of the present work. On the other hand, Boden et al. [13] results' trends for the change in impedance due to different source's position are opposite to those observed in this work, with both higher resistance and reactance observed for the downstream source. This behavior can be related to the different liner geometries considered, since the present work results are for the same liner as in Spillere et al. [18]. More important is to notice that the evidences suggest that the locally reactive assumption made in the duct propagation models may be not correct, since the in-situ technique does not rely on any effect of the liner in the acoustic field that could be affected by possibly ill-posed BCs.

Fig. 16 shows the spatial distribution along the diameter of the central orifice of the first (i.e., cavity No.1) and last cavity (i.e., cavity No.11) of instantaneous vertical velocity with the mean flow field subtracted. The latter is obtained from the time-averaged simulation without acoustics. It is evident that both the inflow and outflow cycles show large differences in amplitude between the first and last cavity depending on the relative direction of the acoustic wave. More important, the differences in amplitude show that velocity induced by the acoustic wave within the cavity varies with the relative direction, thus stressing the relevance of studying and modelling the flow-acoustics interaction.

Overall, the numerical model overestimates the resistance found in the experimental results. This could be a resolution issue. The 25 cells/d lattice resolution delivers good impedance results for the no-flow case in this work, as
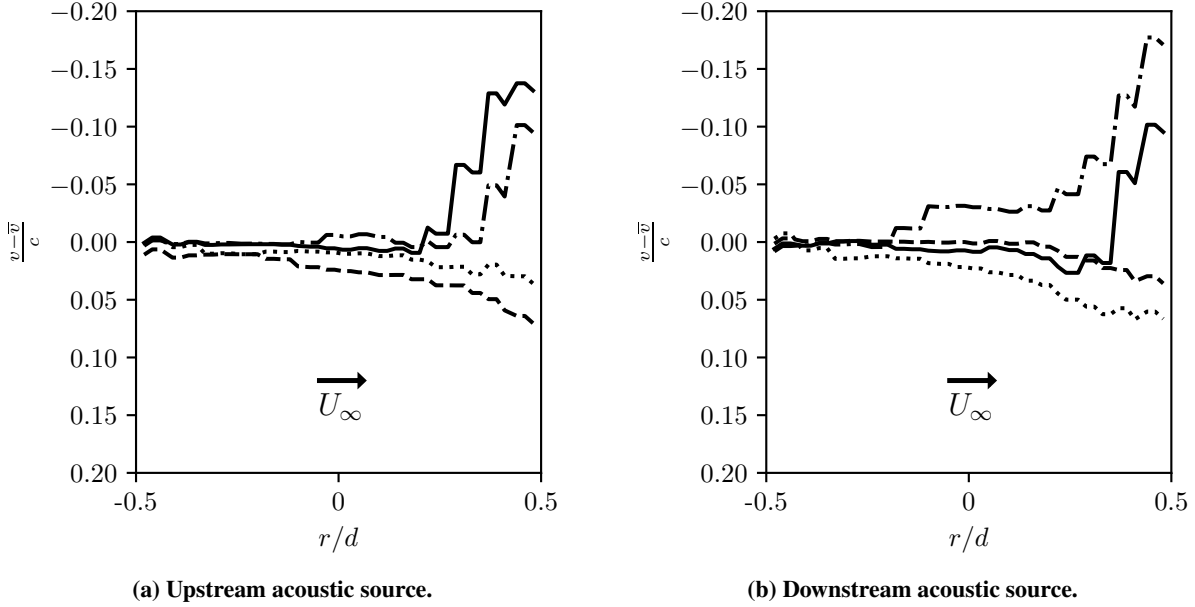
15

(a) Upstream acoustic source.

(b) Downstream acoustic source.

Fig. 16   Velocity profile inside the central orifice of the cavities at $z = 0$**: (—) cavity No.1 [inflow]; (- -) cavity No.1 [outflow]; (- -) cavity No.11 [inflow]; (····) cavity No.11 [outflow]. Data for the 2000 Hz at 145 dB case, with** $M = 0.3$**.**

well as in the work by Schroeder et al. [17]. However, the plots in Figs. 7 and 16 reveal a rather coarse representation of the velocity profile. Also, besides the mismatch to the experimental baselines, undesired oscillations can be seen in the impedance plots of the numerical results, which can be related to the need of a better discretization of the orifice region to adequately represent the flow-acoustics interactions. As a matter of fact, Manjunath et al. [22] results indicate an approximate 40 to 50 cells/d resolution as a reasonable resolution parameter to perform grazing flow simulations. In this work, the resolution effect on the results was not evaluated due to time limitations. The difference of the experimental and numerical flow profiles could also play a role in the mismatch of the numerical model, since the numerical model acoustic results generally overestimate the experimental baseline by an approximate factor 2. Both resolution and flow profile effects need further investigations.

D. Towards the Improvements of the Computational Results

The numerical results shown above report large differences to the experimental ones, particularly with respect to the resistance values. In order to understand the reasons of such discrepancies, studies are ongoing to verify the effect of the grid resolution and the potential improvement of using the legacy solver implemented in PowerFLOW. The latter is known to be less dissipative and more accurate for acoustic simulations, because of a different approach adopted to solve the energy equation. Fig 17 reports the preliminary results of this investigation. The benefits of the legacy solver combined with increased resolution are evident. Similarly to what was reported by Avallone and Damiano [33], using the Dean's method, the numeric results tend to overestimate the resistance and predict a lower reactance in the presence of flow. Furthermore, it is evident that the numerical results using the MM method overestimate largely the resistance with respect to the other two methods. This might be caused by the fact that the model for the modal analysis does not account for the free-slip BC on the wall opposite to the liner. Further analysis will be needed to clarify the limitations and potential improvements of the numerical setup.

V. Conclusions

This paper presented impedance results for a multi-cavity SDOF liner geometry obtained numerically by the in-situ technique, the mode matching method and by a Prony-like KT algorithm. The numerical results were compared to experimental baselines from the UFSC grazing flow impedance test facility. Acoustic simulations for six different frequencies at two SPLs were conducted for the no-flow case and for a maximum Mach number of 0.3 grazing flow case.
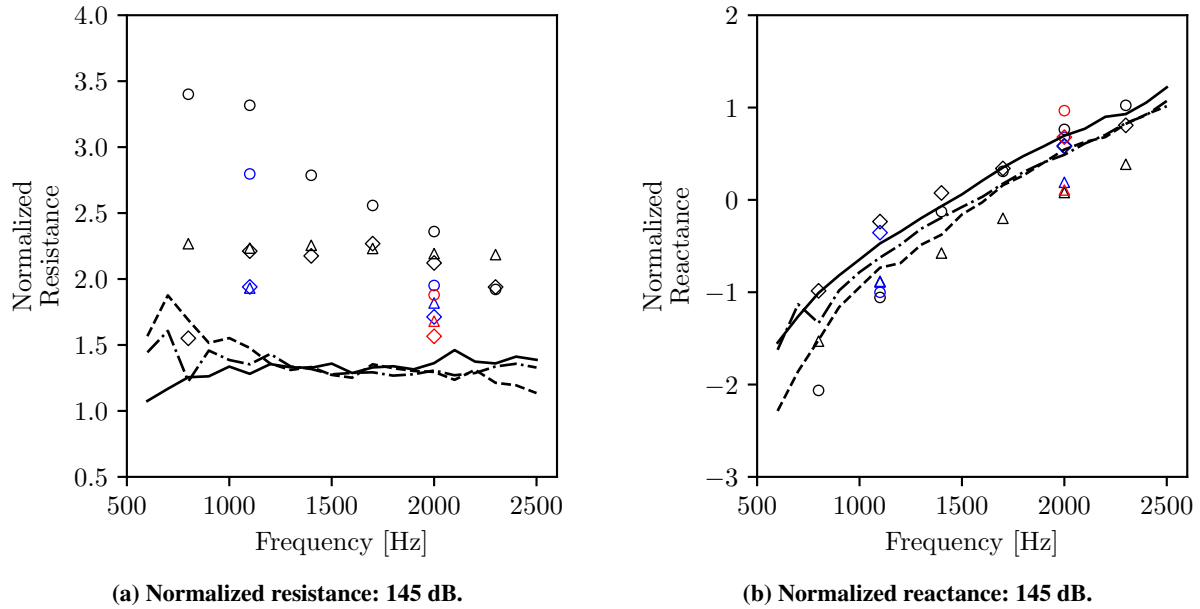
16

(a) Normalized resistance: 145 dB.

(b) Normalized reactance: 145 dB.

Fig. 17 Normalized impedance for the $M = 0.3$ **grazing flow case as a function of the incident acoustic wave frequency (upstream source): (—) experimental [in-situ]; (- -) experimental [MM]; (-·-) experimental [KT]; (△) numerical [in-situ]; (○) numerical [MM]; (◇) numerical [KT]. Colored scatter plots: (black) 25 cells/**d **without legacy solver; (blue) 25 cells/**d **with legacy solver; (red) 50 cells/**d **with legacy solver.**

Both upstream and downstream positioned acoustic sources were considered. The numerical model presented good agreement with experimental data for the no-flow case, considering a 25 cells per orifice diameter meshing scheme. However, large discrepancies were observed between numerical and experimental results for the case with flow. The model seems to be sensitive enough to capture the effects of the grazing flow in the impedance, as well as the difference seen experimentally in both resistance and reactance when the acoustic source's relative position changes from upstream to downstream. Nevertheless, the current model needs further improvement, so as to properly represent the experimental results when grazing flow is present. Particularly, the model overestimates the resistance. The effects of a less dissipative solver, higher resolution and adjusted boundary conditions on the numerical model are being evaluated by ongoing studies. Preliminary results for the less dissipative solver performance and higher resolution meshing schemes were presented, and are much closer to the experimental baseline. Detailed analysis of the flow and the flow-acoustics interactions in the liner will be done in the future, when the model is properly adjusted.

This is the first work to the authors' knowledge to present acoustic results for the same liner geometry obtained by three different methods. A large experimental database is available together with the liner geometry parameters, which can be used in future investigations. All the impedance assessment methods demonstrated to be capable of providing reasonable predictions of the liner's acoustic properties. All of them also exhibit the change in both the predicted resistance and reactance, when the acoustic source's position changes from upstream to downstream. This could mean that the locally reactive assumption, commonly made in lined ducts propagation models, may be not correct, since the in-situ technique does not rely on any possibly ill-posed BCs.

Acknowledgments

17

References

[1] Malmary, C., Carbonne, S., Aurégan, Y., and Pagneux, V., "Acoustic impedance measurement with grazing flow," American Institute of Aeronautics and Astronautics Inc., 2001. https://doi.org/10.2514/6.2001-2193.

[2] Murray, P. B., and Astley, R. J., "Development of a single degree of freedom perforate impedance model under grazing flow and high SPL," 2012. https://doi.org/10.2514/6.2012-2294.

[3] Lafont, V., Méry, F., Reulet, P., and Simon, F., "Surface temperature measurement of acoustic liners in the presence of grazing flow and thermal gradient," *Experiments in Fluids*, Vol. 62, 2021. https://doi.org/10.1007/s00348-021-03184-w.

[4] Tam, C. K., Kurbatskii, K. A., Ahuja, K. K., and Gaeta, R. J., "A numerical and experimental investigation of the dissipation mechanisms of resonant acoustic liners," *Journal of Sound and Vibration*, Vol. 245, 2001, pp. 545–557. https://doi.org/10.1006/jsvi.2001.3571.

[5] Tam, C. K., Ju, H., and Walker, B. E., "Numerical simulation of a slit resonator in a grazing flow under acoustic excitation," *Journal of Sound and Vibration*, Vol. 313, 2008, pp. 449–471. https://doi.org/10.1016/j.jsv.2007.12.018.

[6] Zhang, Q., and Bodony, D. J., "Numerical simulation of two-dimensional acoustic liners with high-speed grazing flow," *AIAA Journal*, Vol. 49, 2011, pp. 365–382. https://doi.org/10.2514/1.J050597.

[7] Tam, C. K., Pastouchenko, N. N., Jones, M. G., and Watson, W. R., "Experimental validation of numerical simulations for an acoustic liner in grazing flow: Self-noise and added drag," *Journal of Sound and Vibration*, Vol. 333, 2014, pp. 2831–2854. https://doi.org/10.1016/j.jsv.2014.02.019.

[8] Zhang, Q., and Bodony, D. J., "Numerical investigation of a honeycomb liner grazed by laminar and turbulent boundary layers," *Journal of Fluid Mechanics*, Vol. 792, 2016, pp. 936–980. https://doi.org/10.1017/jfm.2016.79.

[9] Avallone, F., Manjunath, P., Ragni, D., and Casalino, D., "Lattice-boltzmann very large eddy simulation of a multi-orifice acoustic liner with turbulent grazing flow," American Institute of Aeronautics and Astronautics Inc, AIAA, 2019. https://doi.org/10.2514/6.2019-2542.

[10] Renou, Y., and Aurégan, Y., "Failure of the Ingard–Myers boundary condition for a lined duct: An experimental investigation," *The Journal of the Acoustical Society of America*, Vol. 130, 2011, pp. 52–60. https://doi.org/10.1121/1.3586789.

[11] Ingard, U., "Influence of Fluid Motion Past a Plane Boundary on Sound Reflection, Absorption, and Transmission," *The Journal of the Acoustical Society of America*, Vol. 31, 2005, p. 1035. https://doi.org/10.1121/1.1907805.

[12] Myers, M., "On the acoustic boundary condition in the presence of flow," *Journal of Sound and Vibration*, Vol. 71, No. 3, 1980, pp. 429–434. https://doi.org/10.1016/0022-460X(80)90424-1.

[13] Boden, H., Cordioli, J. A., Spillere, A., and Serrano, P., "Comparison of the effect of flow direction on liner impedance using different measurement methods," *23rd AIAA/CEAS Aeroacoustics Conference*, American Institute of Aeronautics and Astronautics, 2017. https://doi.org/10.2514/6.2017-3184.

[14] Brambley, E. J., "Well-Posed boundary condition for acoustic liners in straight ducts with flow," 2011, pp. 1272–1282. https://doi.org/10.2514/1.J050723.

[15] Aurégan, Y., Starobinski, R., and Pagneux, V., "Influence of grazing flow and dissipation effects on the acoustic boundary conditions at a lined wall," *The Journal of the Acoustical Society of America*, Vol. 109, 2001, pp. 59–64. https://doi.org/10.1121/1.1331678.

[16] Spillere, A. M. N., Bonomo, L. A., Cordioli, J. A., and Brambley, E. J., "Experimentally testing impedance boundary conditions for acoustic liners with flow: Beyond upstream and downstream," *Journal of Sound and Vibration*, Vol. 489, 2020. https://doi.org/10.1016/j.jsv.2020.115676.

[17] Schroeder, L., Spillere, A. M., Bonomo, L. A., da Silva, A. R., Avallone, F., and Cordioli, J. A., "Numerical Investigation of Acoustic Liners Experimental Techniques using a Lattice-Boltzmann Solver," American Institute of Aeronautics and Astronautics (AIAA), 2021. https://doi.org/10.2514/6.2021-2144.

[18] Spillere, A. M., Braga, D. S., Seki, L. A., Bonomo, L. A., Cordioli, J. A., Rocamora, B. M., Greco, P. C., dos Reis, D. C., and Coelho, E. L., "Design of a single degree of freedom acoustic liner for a fan noise test rig," *International Journal of Aeroacoustics*, Vol. 20, 2021, pp. 708–736. https://doi.org/10.1177/1475472X211023831.

[19] Dean, P. D., "An in situ method of wall acoustic impedance measurement in flow ducts," *Journal of Sound and Vibration*, Vol. 34, 1974, pp. 97–IN6. https://doi.org/10.1016/S0022-460X(74)80357-3.

[20] Elnady, T., and Bodén, H., "An Inverse Analytical Method for Extracting Liner Impedance from Pressure Measurements," 2004. https://doi.org/10.2514/6.2004-2836.

[21] Bonomo, L. A., Spillere, A. M., and Cordioli, J. A., "Parametric Uncertainty Analysis for Impedance Eduction Based on Prony's Method," *https://doi.org/10.2514/1.J059071*, Vol. 58, 2020, pp. 3625–3638. https://doi.org/10.2514/1.J059071.

[22] Manjunath, P., Avallone, F., Casalino, D., Ragni, D., and Snellen, M., "Characterization of liners using a lattice-boltzmann solver," American Institute of Aeronautics and Astronautics Inc, AIAA, 2018. https://doi.org/10.2514/6.2018-4192.

[23] Casalino, D., Hazir, A., and Mann, A., "Turbofan broadband noise prediction using the lattice boltzmann method," *AIAA Journal*, Vol. 56, 2018, pp. 609–628. https://doi.org/10.2514/1.J055674.

[24] da Silva, A. R., and Greco, G. F., "Computational investigation of plane wave reflections at the open end of subsonic intakes," *Journal of Sound and Vibration*, Vol. 446, 2019, pp. 412–428. https://doi.org/10.1016/j.jsv.2019.01.044.

[25] Krüger, T., Kusumaatmaja, H., Kuzmin, A., Shardt, O., Silva, G., and Viggen, E. M., *The Lattice Boltzmann Method*, Springer International Publishing, 2017. https://doi.org/10.1007/978-3-319-44649-3.

[26] Succi, S., *The Lattice Boltzmann Equation for Fluid Dynamics and Beyond*, 1$^{\text{st}}$ ed., Clarendon Press, 2001.

[27] Shan, X., Yuan, X. F., and Chen, H., "Kinetic theory representation of hydrodynamics: a way beyond the Navier–Stokes equation," *Journal of Fluid Mechanics*, Vol. 550, 2006, pp. 413–441. https://doi.org/10.1017/S0022112005008153.

[28] Chen, H., Chen, S., and Matthaeus, W., "Recovery of the Navier-Stokes Equations Using a Lattice-Gas Boltzmann Method," *Physical Review A*, Vol. 45, 1992. https://doi.org/10.1103/PhysRevA.45.R5339.

[29] *PowerFLOW 2021 User's Guide*, Dassault Systèmes, 2021.

[30] Habibi, K., Gong, H., Najafiyazdi, A., and Mongeau, L. G., "Prediction of the Sound radiated from Low-Mach Internal Mixing Nozzles with Forced Mixers using the Lattice Boltzmann Method," American Institute of Aeronautics and Astronautics, 2013. https://doi.org/10.2514/6.2013-2143.

[31] Fares, E., "Unsteady flow simulation of the Ahmed reference body using a lattice Boltzmann approach," *Computers and Fluids*, Vol. 35, 2006, pp. 940–950. https://doi.org/10.1016/j.compfluid.2005.04.011.

[32] Teixeira, C. M., "Incorporating Turbulence Models into the Lattice-Boltzmann Method," *International Journal of Modern Physics C*, Vol. 09, No. 08, 1998, pp. 1159–1175. https://doi.org/10.1142/S0129183198001060.

[33] Avallone, F., and Damiano, C., "Acoustic-induced velocity in a multi-orifice acoustic liner grazed by a turbulent boundary layer," American Institute of Aeronautics and Astronautics (AIAA), 2021. https://doi.org/10.2514/6.2021-2169.

[34] Schlichting, H., and Gersten, K., "Internal Flows," *Boundary-Layer Theory*, Springer Berlin Heidelberg, Berlin, Heidelberg, 2017, pp. 519–556.

[35] Levenberg, K., "A method for the solution of certain non-linear problems in least squares," *Quarterly of Applied Mathematics*, Vol. 2, 1944, pp. 164–168. https://doi.org/10.1090/qam/10666.

[36] Marquardt, D. W., "An Algorithm for Least-Squares Estimation of Nonlinear Parameters," *Journal of the Society for Industrial and Applied Mathematics*, Vol. 11, No. 2, 1963, pp. 431–441. https://doi.org/10.1137/0111030.

[37] Dokumaci, E., "Sound transmission in narrow pipes with superimposed uniform mean flow and acoustic modelling of automobile catalytic converters," *Journal of Sound and Vibration*, Vol. 182, No. 5, 1995, pp. 799–808. https://doi.org/10.1006/jsvi.1995.0233.

[38] Jing, X., Peng, S., and Sun, X., "A straightforward method for wall impedance eduction in a flow duct," *The Journal of the Acoustical Society of America*, Vol. 124, 2008, pp. 227–234. https://doi.org/10.1121/1.2932256.

[39] Jones, M. G., Watson, W. R., Parrott, T. L., and Smith, C. D., "Design and evaluation of modifications to the NASA Langley flow impedance tube," 2004, pp. 451–463. https://doi.org/10.2514/6.2004-2837.